C. R. Mecanique 347 (2019) 504–523

Contents lists available at ScienceDirect

Comptes Rendus Mecanique

www.sciencedirect.com

Mass-loss effects on the flow behavior in broken argillaceous red sandstone with different particle-size distributions

Jiangyu Wu [a,b,e], Guansheng Han [a,b,*], Meimei Feng [a,b,*], Hailing Kong [c], Bangyong Yu [d], Luzhen Wang [c], Yuan Gao [a,b]

[a] State Key Laboratory for Geomechanics & Deep Underground Engineering, China University of Mining & Technology, Xuzhou, Jiangsu 221116, China
[b] School of Mechanics & Civil Engineering, China University of Mining & Technology, Xuzhou, Jiangsu 221116, China
[c] College of Civil Engineering, Yancheng Institute of Technology, Yancheng, Jiangsu 224051, China
[d] Institute of Construction Engineering Technology, Changzhou Vocational Institute of Engineering, Changzhou 213164, Jiangsu, China
[e] Nottingham Centre for Geomechanics, Faculty of Engineering, University of Nottingham, University Park, Nottingham NG7 2RD, UK

ARTICLE INFO

Article history:
Received 4 July 2018
Accepted 25 March 2019
Available online 21 June 2019

Keywords:
Mass loss
Broken rock mass
Argillaceous red sandstone
Seepage property
Genetic algorithm

ABSTRACT

Under the action of corrosion, abrasion and erosion of surface water and groundwater, the fine rock particles migrate with water and are gradually lose mass, which seriously deteriorates the internal structure of rock mass, causing seepage disasters. It is important to study the effect of mass loss on the seepage property of a broken rock to understand its engineering behavior. Consequently, an experimental system for testing the seepage property of broken rock under the condition of mass loss was designed, and it also could provide the variations of mass loss and porosity. A genetic algorithm of non-Darcy flow was constructed to characterize the seepage properties of broken rock. The effects of mass conservation and mass loss on the seepage properties of broken rock with different Talbot gradation indices were discussed. The results showed that the migration of fine particles in the internal structure of broken rock caused the fluctuations of permeability parameters even in the case of mass conservation. Under the condition of mass loss, the pore structure and framework structure of broken rock were damaged by the gradual loss of rock particles, which resulted in the gradual variation in the seepage property of broken rock. The broken rock specimen with smaller Talbot gradation index lost more easily rock particles. And the permeability of the broken rock specimen under mass loss was negatively correlated with the Talbot gradation index. It indicated that the broken rock with the finer particles caused more easily an unstable structure.

1. Introduction

Argillaceous red sandstones are widely distributed in southern China, south-central China, and southwestern China. It presents poor engineering behavior in many projects, due to specific properties of easy argillization after contact with water [1]. For example, in Jiangxi, Hunan and other provinces, the frequent occurrences of unstable failures in the construction

* Corresponding authors at: State Key Laboratory for Geomechanics & Deep Underground Engineering, China University of Mining & Technology, Xuzhou, Jiangsu 221116, China.
E-mail addresses: wujiangyu@cumt.edu.cn (J. Wu), han_gs@cumt.edu.cn (G. Han), fengmeimei@cumt.edu.cn (M. Feng).

https://doi.org/10.1016/j.crme.2019.03.014
1631-0721/

of cutting slopes of highways and railways within these mountainous areas with argillaceous red sandstones were easily caused by the actions of surface water and bedrock pore water [2–4]. Landslide caused train derailment, which resulted in 19 people dead and 71 people injured, collapsed mud of more than 8000 m^3 in Jiangxi province on 23 May 2010 [5]. Further, during the tunneling process in these areas, the groundwater and geological structures easily caused disasters such as large deformation of support structure, collapse and water inrush [6–8]. In addition, in the process of underground mining, the water flowing fractured zone (channels) fully developed under disturbance, which resulted in groundwater within argillaceous red sandstone strata rushing into the working face [9,10].

Therefore, lots of experimental researches on the intact rock specimens were carried out to investigate the physical and mechanical properties of the argillaceous red sandstone [11–14], which provided some valuable conclusions [15–17]. For example, Baud et al. revealed the impact mechanism of water-weakening on the strength of sandstone in the cataclastic flow regime [18]. Sulem and Ouffroukh studied the relation between the hydromechanical behavior of the sandstone specimen and the confining pressure [19]. It was generally considered that water not only accelerated to fracture the cohesive particles of the rock material under loading, but also weakened the friction effect among the internal grains [20,21]. In fact, most argillaceous rocks were easily slimed, disintegrated and broken to form the broken rock after contacting with water, which resulted in significant differences in the mechanical properties of broken rock and intact ones, which are mainly present in permeability, so that it is necessary to investigate the seepage properties of argillaceous red sandstone further.

At present, abundant permeability experiments were carried out to investigate the seepage properties of broken rock [22]. Liu et al. [23] studied the effects of the axial stress on the permeability coefficients of broken rock by the steady-state seepage method. Due to the fact that the seepage behavior of broken rock manifested itself as a more pronounced nonlinear flow [24], Miao et al. established non-linear dynamic equations for a non-Darcy flow in broken rock based on the experimental results, and obtained the solution diagram for a steady-state flow under specific boundary conditions through a dimensionless transformation [25]. In addition, Miao et al. and Kong et al. investigated the relations between the non-Darcy flow parameters (permeability k, non-Darcy flow β factor, and acceleration coefficient c_a) and the porosity and particle size of broken rock [26,27]. The non-Darcy flow properties of broken rock are not only related to the porosity of the broken rock, but also related to the lithology of the rock [28]. Thus, Ma et al. tested the seepage properties of crushed mudstone, limestone, and sandstone specimens with variable particle sizes under different porosities [29].

However, the above studies mainly discussed the influences of lithology, porosity, and particle size on the seepage property of broken rock under the condition of mass conservation, i.e. both sides of the specimen covered with felts or filter cloths in the seepage experiments. The aim was to prevent the loss of rock and soil particles, and the permeability parameters were obtained from these experiments as the basic parameters of geomaterials. But this method is not suitable for characterizing the engineering rock and soil mass with the existence of mass loss. For example, in the argillaceous red sandstone areas, the rock masses have the specific characteristics of easy argillization after contact with water and disintegration under disturbance. The stress field, seepage field, fracture network and channels of this specific rock mass vary significantly under the impact of the external load with corrosion, abrasion, and erosion by surface water and groundwater [30–34]. The mudding rock particles and fine grains form a two-phase fluid with water; the solid particles migrate in the cracks of the rock mass and gradually loose mass [35–38]. It greatly deteriorates the structure of the rock mass, which easily results in seepage disasters [39]. Hence, a system for testing the seepage property of broken rock under the condition of mass loss was designed. And there are multiple factors that can affect the seepage properties of the broken rock, among which, the quantization of particle size distribution being the most difficult one [40]. This is because the multiple mass ratios of broken rocks with different particles sizes constitute a high-dimensional parameter space, which results in the curse of dimensionality. It causes the quick loss of small particles in broken rock within a short time, with the result that particle collection and mass loss are difficult to obtain accurately. Consequently, Talbot's gradation theory was used to describe the particle size distribution of broken rock, which not only could overcome the curse of dimensionality but also be similar to broken rock in engineering [41]. The experiment was carried out to obtain the seepage properties of broken rock by using the self-made seepage test system. Based on our experimental results, a genetic algorithm of non-Darcy flow conform to the seepage behavior of broken rock was established. The effects of mass conservation and mass loss on the porosity and seepage property of broken rock with different Talbot gradation indices were discussed.

2. Materials and methods

2.1. Experimental material

In this test, the argillaceous red sandstone samples were obtained from the −473 m heading face of a coal mine in China. Fig. 1 presents the X-ray diffraction (XRD) pattern of argillaceous red sandstone. It can be seen that the rock sample contains strong hydrophilic clay minerals, such as kaolinite. The pores, microcracks and original fissures in the rock are easily propagated after immersing into the water. The kaolinite easily combines with water molecules ($Al_4Si_4O_{10}(OH)_8 + nH_2O \rightarrow Al_4Si_4O_{10}(OH)_8 \cdot nH_2O$), which causes the expansion and deformation of particle volume, cracking and disintegration in rock [42]. Table 1 shows the main physical properties of argillaceous red sandstone.

Table 1
Physical properties of argillaceous red sandstone.

Natural density (g/cm^3)	Saturated density (g/cm^3)	Dry density (g/cm^3)	Saturated water content (%)	Porosity	Uniaxial compressive strength (MPa)	Elastic modulus (GPa)
2.07	2.10	2.05	2.38	0.05	47.79	6.38

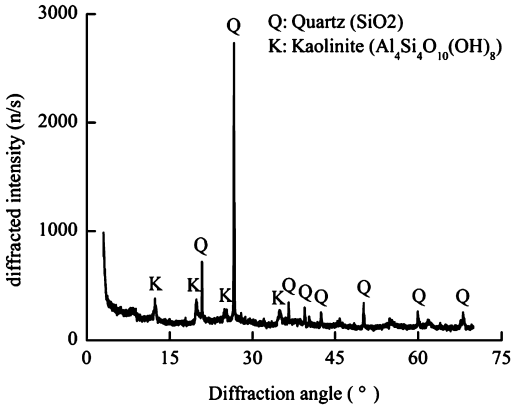

Fig. 1. XRD spectrum of argillaceous red sandstone.

Fig. 2. Broken argillaceous red sandstone in different particle sizes.

2.2. Preparation of broken rock specimens

In order to eliminate the influence of the size effect of the particle on the test results, the American Society for Testing and Materials (ASTM) considered that the maximum particle size should not exceed one third of the cylinder diameter of the specimen [43], and the previous studies suggested that the cylinder diameter should be set to the maximum particle size five times [44]. The internal diameter of the permeameter was 100 mm, so the maximum particle size of the rock used in this experiment was 20 mm. The argillaceous red sandstones were crushed into six particle size intervals of (0–2 mm), (2–5 mm), (5–8 mm), (8–10 mm), (10–15 mm), and (15–20 mm) as shown in Fig. 2. However, the mass distributions of

Table 2
Mass distribution (%) of rock particles under different Talbot indices.

Talbot index	0–2 mm	2–5 mm	5–8 mm	8–10 mm	10–15 mm	15–20 mm
0.3	50.12	15.86	9.99	5.26	10.50	8.27
0.5	31.62	18.38	13.25	7.46	15.89	13.40
0.7	19.95	17.94	14.76	8.91	20.20	18.24
0.9	12.59	16.13	15.12	9.75	23.60	22.81

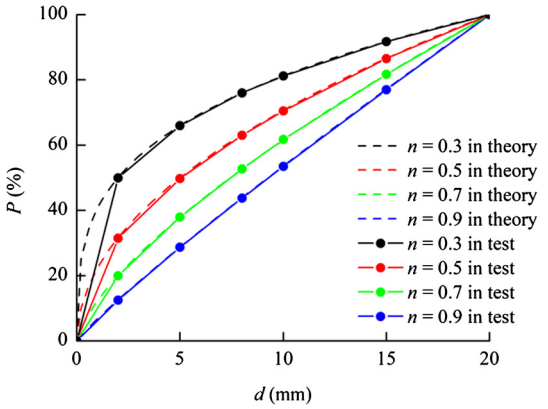

Fig. 3. Talbot's gradation curves of broken rock.

rock particles with multiple particle sizes easily constitute a high-dimensional parameter space. It is difficult to evaluate the effect of the particle size distribution of broken rock on the test results. Consequently, Talbot's gradation theory was used to describe the particle size distribution of broken rock, which not only could overcome the curse of dimensionality, but also be similar to broken rock in engineering.

Talbot's gradation proposed the following formula:

$$P = \frac{M}{M_t} = \left(\frac{d}{D}\right)^n \times 100\% \tag{1}$$

where d is the particle size of broken rock, mm; D is the maximum particle size of broken rock, mm; n is the Talbot index; P is the percentage of broken rock which the particle size less than or equal to d; M is the mass of broken rock which the particle size less than or equal to d, g; M_t is the total mass of broken rock specimen, g.

The mass of particle size in the interval $[d_1, d_2]$ can be calculated according to Eq. (1):

$$M_{d_1}^{d_2} = \left[\left(\frac{d_2}{D}\right)^n - \left(\frac{d_1}{D}\right)^n\right] M_t \tag{2}$$

where $M_{d_1}^{d_2}$ is the mass of broken rock which the particle size in the interval of $[d_1, d_2]$, g.

Equation (2) is a greatly significant continuous gradation to determine the range of rock particles. The arbitrary value of the continuous grading index n is usually given to obtain the experimental results in detail. The broken rock specimens with different particle sizes were obtained by adopting different values of n.

Table 2 lists the mass distribution of rock particles in the broken rock specimens under different Talbot indices, Fig. 3 shows the percentage of rock particles in each particle size, under the conditions of theory and test. The total weight of the individual broken rock specimen was 2000 g. As can be seen from the table and figure, the content of fine particles is negatively related to Talbot's gradation index.

2.3. Experimental system and process

The experimental system for testing the seepage property of broken rock under the condition of mass loss was designed as shown in Fig. 4, which is comprised of five parts: (**A**) Load and control system of hydraulic pressure, (**B**) load and control system of the axial displacement, (**C**) permeability system, (**D**) data acquisition and analysis system, and (**E**) particle collection system.

A. A load and control system of hydraulic pressure, consisting of a dual-acting hydraulic cylinder, an oil pump system, and a water pump. It can provide adjustable and stable permeability pressure and simulate the hydraulic pressure in engineering. The main principle is the use of a water pump to fill the dual-acting hydraulic cylinder with water, and a stable hydraulic pressure from the double-acting hydraulic cylinder can be provided by the stable oil pressure from the oil pump system. The reason for this is that it can ensure adequate water supply, and the seepage test does not need to be interrupted.

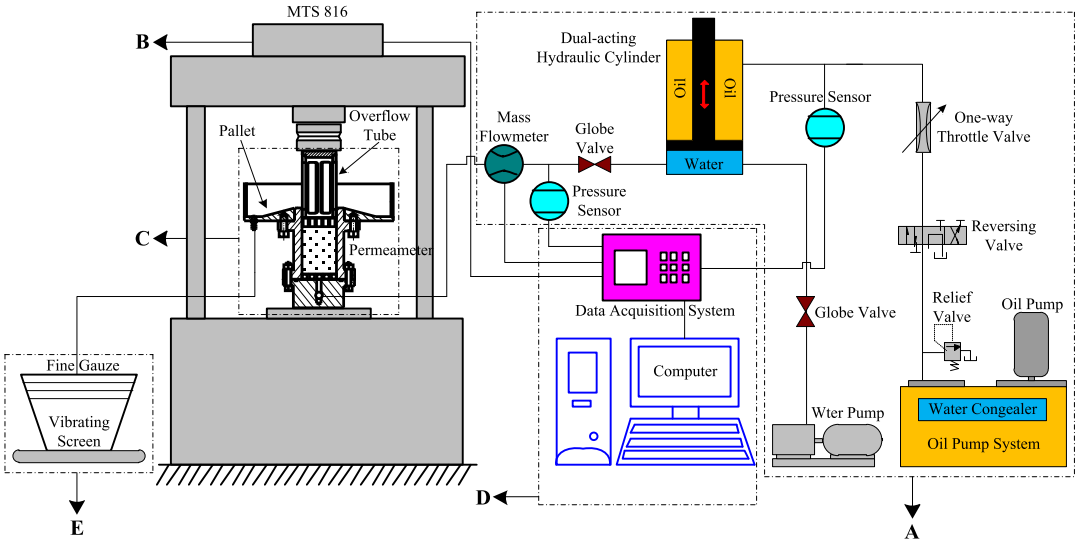

Fig. 4. Experimental system.

B. A load and control system of axial displacement, including an MTS 816 rock mechanics test system and indenters. The height of the broken rock specimen is controlled by the displacement or force control method, and the initial porosity of the specimen is calculated to simulate the porosity of broken rock in engineering.

C. A permeability system, consisting of a permeameter, a pallet, and an overflow tube. It bestows the advantage of openness and can be used for testing the seepage property of broken rock with rock particles migration and loss. If the felts are capped at both sides of the permeameter, the seepage property of broken rock under the condition of mass conservation can also be tested.

D. A data acquisition and analysis system, including a pressure sensor, a mass flowmeter, a data acquisition system, and a computer. It is used for the real-time collection of hydraulic pressure, oil pressure, flow rate, axial stress, and axial displacement in the experiment.

E. A particle collection system, consisting of a vibrating screen, a fine gauze, and an electronic balance. It is used to filter the mixture containing water and rock particles, and to collect the migrated and lost rock particles outflowed from the broken rock specimen.

The prepared broken rock specimen was mixed evenly into the permeameter to measure the height h' under the natural accumulation state. The MTS816 was controlled to load the broken rock specimen and compress the axial displacement Δh to obtain the initial height h_0 and the initial porosity ϕ_0 and keep this displacement immovable. The seepage test system was adjusted to set the initial hydraulic pressure to carry out the seepage experiment on the broken rock specimen. The sampling time of this system was set as 1 s, then the time series of permeability pressure p and flow rate Q could be obtained. It should be noted that a pallet was designed to connect the permeameter and the vibrating screen instead of using a pipe, which could avoid the clogging and residue of the gushing rock in the pipe. The lost rock particles were collected every minute by using a gauze in the seepage experiment under the condition of mass loss. In mass conservation conditions, the felts were covered on both sides of the specimen to prevent the loss of rock particles.

3. Calculation theories

3.1. Calculation of mass loss

The rock particles outflowed with water and were collected every Δt in the experiment. After drying and weighting, the masses $m_1, m_2, \ldots, m_i$ of rock particles were obtained at each time interval. The mass-loss rate v_m and the total loss mass m_t during each time period can be calculated by:

$$v_\mathrm{m} = \frac{m_i}{\Delta t} \tag{3}$$

$$m_t = m_1 + m_2 + m_3 + \cdots + m_i \tag{4}$$

3.2. Calculation of porosity

The mass density of rock is ρ_z and the total mass of the rock specimen is m_z, then the volume of the intact rock specimen can be obtained by:

$$V_z = \frac{m_z}{\rho_z} \tag{5}$$

The broken rock specimen was well distributed in the permeameter to measure the height h'. After the compression of Δh, the initial height of the broken rock specimen can be calculated by:

$$h_0 = h' - \Delta h \tag{6}$$

Therefore, the initial porosity ϕ_0 of the broken rock specimen before seepage is:

$$\phi_0 = \frac{V' - V_z}{V'} = \frac{\pi a^2 h_0 - V_z}{\pi a^2 h_0} \tag{7}$$

where V' is the volume of the broken rock specimen after compression, a is the internal radius of the permeameter.

During the seepage process, the height of the broken rock specimen was unvaried. Therefore, it is assumed here that the volume of the specimen after compression does not change. The migration and loss of rock particles cause the mass loss of broken rock, which results in a variation of porosity in the specimen. The varied porosity $\Delta\phi_t$ of the broken rock specimen can be obtained from the lost mass m_i in any time period as follows:

$$\Delta\phi_t = \frac{m_i}{V'\rho_z} \tag{8}$$

Then the porosity ϕ_t of the broken rock specimen and its variation rate v_ϕ in each time period can be obtained as:

$$\phi_t = \phi_0 + \frac{1}{V'\rho_z}(m_1 + m_2 + m_3 + \cdots + m_i) \tag{9}$$

$$v_\phi = \frac{\phi_{t+1} - \phi_t}{\Delta t} \tag{10}$$

3.3. Calculation of permeability parameters

The seepage process of broken rock follows the momentum equation of the non-Darcy flow [45]:

$$\rho_l c_a \frac{\partial \vec{V}}{\partial t} = -\nabla p - \frac{\mu_0}{k}\vec{V} - \rho_l \beta \vec{V}^2 + \rho_l g \nabla z \tag{11}$$

where ρ_l is the density of the fluid, kg/m^3, c_a is the acceleration coefficient of fluid (dimensionless), $\vec{V}$ is the seepage velocity of the fluid, m/s, p is the permeability pressure, MPa, ∇p is the pressure gradient of fluid, MPa/m, μ_0 is the dynamic viscosity of fluid, Pa s, k is the non-Darcy flow permeability, m^2, β is the non-Darcy factor, m^{-1}. ∇z is the unit vector in the direction of gravity.

The action of gravity can be ignored, because it is much smaller than the hydraulic pressure. In the test, the water flows into the permeameter from the inlet pipe, and then outflows from the outlet pipe after the flow through the broken rock specimen, so the seepage in the specimen can be simplified as the one-dimensional single-phase non-Darcy flow; the momentum conservation relation can be rewritten as:

$$\rho_l c_a \frac{\partial V}{\partial t} = -\frac{\partial p}{\partial z} - \frac{\mu_0}{k}V - \rho_l \beta V^2 \tag{12}$$

where z is the coordinate of gravity direction, and the seepage velocity V can be obtained from the flow rate, $V = \frac{Q}{\pi a^2}$.

In general, the permeability parameters of geomaterials can be obtained according to Eq. (12) [46,47]. However, taking into account the effects of particle migration and mass loss on the broken rock, its internal structure and fracture network are varying over time. Thus, the permeability parameters also vary with time. For this purpose, a systematical method needs to be constructed for calculating the time-varying permeability parameters of the broken rock.

At the sampling time $t_i = i\tau$, $(i = 0, 1, 2, \ldots, N)$, the expression can be obtained from the expansion of Eq. (12):

$$\rho_l c_{at_i} a_{t_i} = -G_{pt_i} - \frac{\mu_0}{k_{t_i}} V_{t_i} - \rho_l \beta_{t_i} V_{t_i}^2 \quad (i = 0, 1, 2, \ldots, N) \tag{13}$$

where $a_{t_i} = \frac{\partial V}{\partial t}|_{t_i = i\tau}$ is the local derivative of the seepage velocity at time $t_i = i\tau$, $G_{pt_i} = \frac{\partial p}{\partial z}|_{t_i = i\tau}$.

According to a large number of tests and literature articles [4,22,27,37,40], the relation among the parameters of permeability k, the non-Darcy flow β factor, and the acceleration coefficient c_a satisfies the exponential function:

$$\begin{cases} k_{t_i} = k_r \left(\dfrac{\phi}{\phi_r}\right)^{m_k} \\ \beta_{t_i} = \beta_r \left(\dfrac{\phi}{\phi_r}\right)^{m_\beta} \\ c_{at_i} = c_{ar} \left(\dfrac{\phi}{\phi_r}\right)^{m_c} \end{cases} \tag{14}$$

where k_r, β_r and c_{ar} are the parameters of permeability, the non-Darcy flow factor, and the acceleration coefficient of the specimen under the porosity ϕ_r, m_k, m_β and m_c are the exponential factors. The parameters of k_r, β_r, c_{ar}, m_k, m_β and m_c can be optimized by using the genetic algorithm.

Based on the time series V_{t_i}, $(i = 0, 1, 2, \ldots, N)$ and G_{pt_i}, $(i = 0, 1, 2, \ldots, N)$, the permeability k_{t_i}, the non-Darcy flow factor β_{t_i}, and the acceleration coefficient c_{at_i} at the sampling time $t_i = i\tau$ $(i = 0, 1, 2, \ldots, N)$ can be obtained by using Equations (13) and (14).

Equation (14) can be rewritten as:

$$\begin{cases} \beta_{t_i} = \beta_r \left(\dfrac{k_{t_i}}{k_r}\right)^{n_\beta} \\ c_{at_i} = c_{ar} \left(\dfrac{k_{t_i}}{k_r}\right)^{n_c} \end{cases} \tag{15}$$

where $n_\beta = m_\beta / m_k$, $n_c = m_c / m_k$.

Then Eq. (15) is substituted into Eq. (13),

$$\rho_l c_{ar} \left(\frac{k_{t_i}}{k_r}\right)^{n_c} a_{t_i} = -G_{pt_i} - \frac{\mu_0}{k_i} V_{t_i} - \rho_l \beta_r \left(\frac{k_{t_i}}{k_r}\right)^{n_\beta} V_{t_i}^2 \quad (i = 0, 1, 2, \ldots, N) \tag{16}$$

Equation (16) is an algebraic equation, whose root can be obtained by using numerical methods such as the dichotomy and Newton tangent method, and the root is the estimate of permeability k_{t_i} $(i = 0, 1, 2, \ldots, N)$. It should be noted that the iteration can be stopped when the absolute error of iteration values between the $(n+1)$th and (n)th is less than or equal to 0.001 in the calculation of permeability by using the Newton tangent method, that is, it is considered to converge when $|f(x_{n+1}) - f(x_n)| \leq 0.001$. Using Eq. (15), the estimate of the non-Darcy flow factor β_{t_i}, $(i = 0, 1, 2, \ldots, N)$ and acceleration coefficient c_{at_i}, $(i = 0, 1, 2, \ldots, N)$ also can be obtained.

The authenticities of permeability parameters calculated by Equations (15) and (16) are depending on the rationality of the parameters k_r, β_r, c_{ar}, n_β, and n_c. Consequently, a genetic algorithm is constructed to optimize the above decision parameters [48], as follows.

(1) The first step is to construct the time series of pressure gradient, seepage velocity, and seepage acceleration.

In the seepage experiment, Q_{t_i}, $(i = 0, 1, 2, \ldots, N)$ is the time series of flow rate and p_{t_i}, $(i = 0, 1, 2, \ldots, N)$ is the time series of hydraulic pressure at the sampling time $t_i = i\tau$, $(i = 0, 1, 2, \ldots, N)$ with $\tau = 1$ s. The time series of pressure gradient, seepage velocity, and seepage acceleration can be obtained:

$$G_{pt_i} = \frac{p_{t_i}}{h_0}, \quad (i = 0, 1, 2, \ldots, N) \tag{17}$$

$$V_{t_i} = \frac{Q_{t_i}}{\pi a^2}, \quad (i = 0, 1, 2, \ldots, N) \tag{18}$$

$$a_{t_i} = \frac{V_{t_{i+1}} - V_{t_i}}{\tau}, \quad (i = 0, 1, 2, \ldots, N) \tag{19}$$

(2) The second step consists in producing the coding method.

The interval of the decision parameters should be determined,

$$k_r \in [k_{r1}, k_{r2}] \tag{20}$$

$$\beta_r \in [\beta_{r1}, \beta_{r2}] \tag{21}$$

$$c_{ar} \in [c_{ar1}, c_{ar2}] \tag{22}$$

$$n_\beta \in [n_{\beta 1}, n_{\beta 2}] \tag{23}$$

$$n_c \in [n_{c1}, n_{c2}] \tag{24}$$

The five decision parameters of k_r, β_r, c_{ar}, n_β, and n_c should be transformed into the bit string with the length of 6 consisted of the characters 0 and 1, such as $I_{11} I_{12} \cdots I_{16}$, $I_{21} I_{22} \cdots I_{26}$, $I_{31} I_{32} \cdots I_{36}$, $I_{41} I_{42} \cdots I_{46}$, $I_{51} I_{52} \cdots I_{56}$ and $I_{61} I_{62} \cdots I_{66}$. This completes the code of the binary bit string on the decision parameters.

Then the individual genotype of the genetic algorithm is constituted by using the binary bit string $I_1 I_2 \cdots I_{30}$ with the length of $6+6+6+6+6=30$, the corresponding phenotype of an individual gene being:

$$k_r = k_{r1}\left[\exp\frac{\ln\frac{k_{r2}}{k_{r1}}}{2^6-1}\right]^j, \quad j=\sum_{i=1}^{6}2^i I_{1i} \tag{26}$$

$$\beta_r = \beta_{r1}\left[\exp\frac{\ln\frac{\beta_{r2}}{\beta_{r1}}}{2^6-1}\right]^j, \quad j=\sum_{i=1}^{6}2^i I_{2i} \tag{27}$$

$$c_{\mathrm{ar}} = c_{\mathrm{ar}1}\left[\exp\frac{\ln\frac{c_{\mathrm{ar}2}}{c_{\mathrm{ar}1}}}{2^6-1}\right]^j, \quad j=\sum_{i=1}^{6}2^i I_{3i} \tag{28}$$

$$n_\beta = n_{\beta 1}\left[1+\frac{j}{2^6-1}\frac{n_{\beta 2}-n_{\beta 1}}{n_{\beta 1}}\right], \quad j=\sum_{i=1}^{6}2^i I_{4i} \tag{29}$$

$$n_c = n_{c1}\left[1+\frac{j}{2^6-1}\frac{n_{c2}-n_{c1}}{n_{c1}}\right], \quad j=\sum_{i=1}^{6}2^i I_{5i} \tag{30}$$

(3) The third step is to establish the initial population generation.

The scale of the initial population must be determined first. The number of the binary bit strings in the initial population is defined as ξ_{group}. The last binary bit string in the initial population is defined as k_{group}. In this study, $k_{\mathrm{group}}=\xi_{\mathrm{group}}=100$. The random seeds η should be generated secondly.

Then the binary bit strings with the length of 30 can be generated, which allows us to obtain the initial population:

$$\text{Initial population} = \left\{I_1^i I_2^i \cdots I_{30}^i \middle| i=1,2,\ldots,k_{\mathrm{group}}\right\} \tag{31}$$

(4) The fourth step consists in calculating the numerical solution of permeability parameters.

Each individual chromosome$(i)=I_1^i I_2^i \cdots I_{30}^i$, $(i=1,2,\ldots,k_{\mathrm{group}})$ in the initial population is decoded to obtain the phenotype of an individual gene, and the values of the decision parameters are obtained from Equations (26) to (30).

The permeability, the non-Darcy flow β factor, and the acceleration coefficient of each individual are obtained by using the Newton tangent method according to the time series of the pressure gradient G_{pt_i} and the seepage velocity V_{t_i}. The corresponding time series of permeability, non-Darcy flow β factor and acceleration coefficient are obtained for each individual:

$$k_{t_i} \quad (i=0,1,2,\ldots,N) \tag{32}$$

$$\beta_{t_i} \quad (i=0,1,2,\ldots,N) \tag{33}$$

$$c_{\mathrm{at}_i} \quad (i=0,1,2,\ldots,N) \tag{34}$$

Then the external function of Eq. (12) is constructed. The numerical solution to Eq. (12) is obtained by the fourth-order Runge–Kutta method with variable step size, and it needs to construct the values of pressure gradient, permeability, non-Darcy flow β factor, and acceleration coefficient at the non-sampling time (e.g., $t=2.2\tau$). In the program of the fourth-order Runge–Kutta method with variable step size, the external function needs to call the Lagrange interpolation program of unequal equidistant three-node in the whole interval to interpolate for the pressure gradient, permeability, non-Darcy flow β factor, and acceleration coefficient. For example, at time $t\in(t_i,t_{i+2})$,

$$k = k_{t_i}\frac{(t-t_{i+1})(t-t_{i+2})}{(t_i-t_{i+1})(t_i-t_{i+2})} + k_{t_{i+1}}\frac{(t-t_i)(t-t_{i+2})}{(t_{i+1}-t_i)(t_{i+1}-t_{i+2})} + k_{t_{i+2}}\frac{(t-t_i)(t-t_{i+1})}{(t_{i+2}-t_i)(t_{i+2}-t_{i+1})} \tag{35}$$

$$\beta = \beta_{t_i}\frac{(t-t_{i+1})(t-t_{i+2})}{(t_i-t_{i+1})(t_i-t_{i+2})} + \beta_{t_{i+1}}\frac{(t-t_i)(t-t_{i+2})}{(t_{i+1}-t_i)(t_{i+1}-t_{i+2})} + \beta_{t_{i+2}}\frac{(t-t_i)(t-t_{i+1})}{(t_{i+2}-t_i)(t_{i+2}-t_{i+1})} \tag{36}$$

$$c_{\mathrm{a}} = c_{\mathrm{at}_i}\frac{(t-t_{i+1})(t-t_{i+2})}{(t_i-t_{i+1})(t_i-t_{i+2})} + c_{\mathrm{at}_{i+1}}\frac{(t-t_i)(t-t_{i+2})}{(t_{i+1}-t_i)(t_{i+1}-t_{i+2})} + c_{\mathrm{at}_{i+2}}\frac{(t-t_i)(t-t_{i+1})}{(t_{i+2}-t_i)(t_{i+2}-t_{i+1})} \tag{37}$$

$$G_p = G_{pt_i}\frac{(t-t_{i+1})(t-t_{i+2})}{(t_i-t_{i+1})(t_i-t_{i+2})} + G_{pt_{i+1}}\frac{(t-t_i)(t-t_{i+2})}{(t_{i+1}-t_i)(t_{i+1}-t_{i+2})} + G_{pt_{i+2}}\frac{(t-t_i)(t-t_{i+1})}{(t_{i+2}-t_i)(t_{i+2}-t_{i+1})} \tag{38}$$

The numerical solution to Eq. (12) can be calculated by using the fourth-order Runge–Kutta method with variable step size with the step size of τ. Then the time series of the calculated values of seepage velocity can be obtained:

$$V'_{t_i}, \quad (i=0,1,2,\ldots,N) \tag{39}$$

(5) The fifth step is to calculate the fitness.

The error E_{rr} between the numerical solution of seepage velocity V'_{t_i}, $(i = 0, 1, 2, \ldots, N)$ and the test data V_{t_i}, $(i = 0, 1, 2, \ldots, N)$ must be considered.

$$E_{rr} = \frac{1}{N}\sum_{i=1}^{n}\left(1 - \frac{V'_{t_i}}{V_{t_i}}\right)^2 \tag{40}$$

The fitness function must be constructed and the fitness of every individual in the initial population can be calculated,

$$\mathrm{fitn}(i) = \frac{1}{E_{rr}}, \quad (i = 1, 2, \ldots, k_{\mathrm{group}}) \tag{41}$$

(6) The sixth step consists in selecting the individuals with the mating right.

The $k_{\mathrm{cop}} = \xi_{\mathrm{cop}} = 60$ individuals with mating rights are selected from the initial population by using the random ergodic method. The individual genotype is

$$\mathrm{P_{cop}} = \left\{ \mathrm{chromosome}(i_{\mathrm{c}}) \middle| \, \mathrm{chromosome}(i_{\mathrm{c}}) = I_1^{i_{\mathrm{c}}} I_2^{i_{\mathrm{c}}} \cdots I_{30}^{i_{\mathrm{c}}}, i_{\mathrm{c}} = 1, 2, \ldots, k_{\mathrm{cop}} \right\} \tag{42}$$

(7) The seventh step is to interlace the individuals.

A pair of individuals in $\mathrm{P_{cop}}$ are randomly matched, that is, each gene bit string is randomly generated for each cross bit string, and each pair of cross individuals (couples) is interlaced by a certain crossover probability $p_{\mathrm{c}} = \xi_{\mathrm{c}} = 0.4$ to obtain an individual set $\mathrm{P'_{cop}}$.

(8) The eighth step consists in mutating the individuals.

The mutation bit string of each gene in $\mathrm{P'_{cop}}$ is randomly generated, and the mutation operation is performed for each individual according to a certain mutation probability $p_{\mathrm{m}} = \xi_{\mathrm{m}} = 0.3$. The new population is:

$$\text{New population} = \left\{ I_1^i I_2^i \cdots I_m^i \middle| i = 1, 2, \ldots, k_{\mathrm{cop}} \right\} \tag{43}$$

(9) The ninth step is to set the condition of stop breeding.

The fitness of each individual in the new generation of the population is calculated. If the maximum of fitness is greater than or equal to the pre-set value of $\xi_{\mathrm{s}} = 100$, i.e.:

$$\mathrm{fitn}(i)_{\max} \geq \xi_{\mathrm{s}}, \quad (i = 1, 2, \ldots, k_{\mathrm{cop}}) \tag{44}$$

Or the breeding algebra is equal to the pre-set integer of $N_{\mathrm{g}} = \xi_{\mathrm{g}} = 1001$, then it stops breeding. If $\mathrm{fitn}(i)_{\max} < \xi_{\mathrm{s}}$, the operation is continued until Eq. (44) is satisfied.

The optimal individual (the individual with the greatest fitness) is decoded, that is, the genotypes are transformed into phenotypes according to Equations (26)–(30), and the optimal values of k_r, β_r, c_{ar}, n_β and n_c are obtained. The optimal values of k_r, β_r, c_{ar}, n_β and n_c are substituted into Eq. (16), the permeability k is calculated by using the Newton tangent method at each sampling time, and the non-Darcy flow β factor and the acceleration coefficient c_{a} are obtained from Eq. (15). In summary, the time series of all permeability parameters are obtained.

4. Experimental results

4.1. Mass-loss effects on porosity

Fig. 5 plots the loss mass–time variation curves of broken rock specimens with different Talbot gradation indices; the curves can be described by an exponential function. And the fitting relationships between loss mass and time are presented in Table 3, all the correlation coefficients are more than 0.9. The loss of rock particles inevitably causes the variation of the internal pore structure of broken rock; therefore, Fig. 6 shows the porosity–time variation curves of broken rock specimens with different Talbot gradation indices, which can also be characterized by an exponential function. The fitting relationships are listed in Table 4, all the correlation coefficients are more than 0.9. It can be seen from the figures and tables that the loss of rock particles causes the increase of the porosity of the broken rock, which easily damages the original pore structure and framework structure of rock specimen and expands the channels inside the broken rock. It is noteworthy that the broken rock specimen with smaller Talbot gradation index loses more easily rock particles, and there are peaks in the mass-loss rate and the porosity variation rate as shown in Figs. 7 and 8. It is not difficult to find out that the time at which the mass-loss rate and porosity variation rate reach peaks constantly increase with the Talbot gradation index. This is due to the fact that the broken rock specimen with smaller Talbot gradation index contains more fine rock particles, which cannot be easy to form a stable water-blocking structure. And too much fine rock particles are easily outflowed with water, which results in damage to the internal structure of the broken rock specimen. When the internal structure is damaged to a certain extent, it cannot be enough to withstand the current conditions of external load and water erosion and then instantaneously fail. A large number of rock particles burst out with water immediately, the seepage instability occurs, and the channels of water inrush are formed in the broken rock. Thereafter, the residual rock particles in the specimen gradually outflow with water, and the mass-loss rate and porosity variation rate gradually decrease.

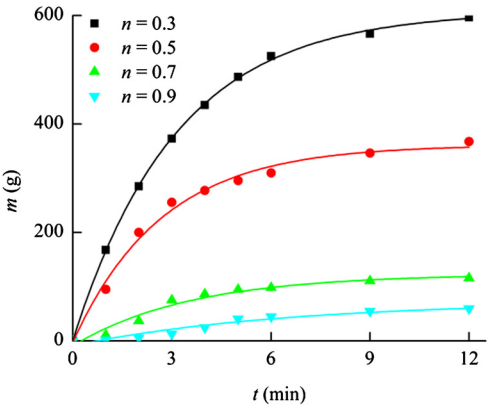

Fig. 5. Relation between loss mass and time.

Table 3
Fitting relationship between loss mass and time.

Talbot index	Fitting relation	Correlation coefficient
0.3	$m = -607.5744e^{-0.3191t} + 607.6217$	0.9995
0.5	$m = -364.0390e^{-0.3705t} + 361.2814$	0.9897
0.7	$m = -132.2898e^{-0.2789t} + 123.1408$	0.9541
0.9	$m = -81.3879e^{-0.1546t} + 72.7097$	0.9287

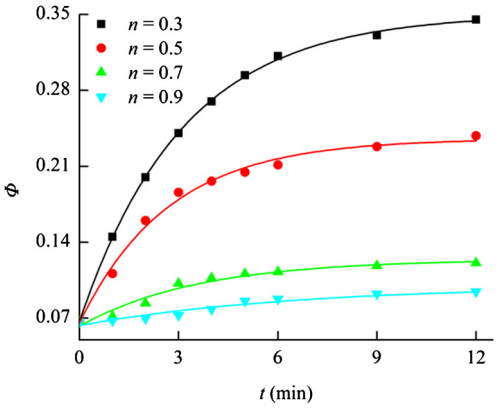

Fig. 6. Relation between porosity and time.

Table 4
Fitting relationship between porosity and time.

Talbot index	Fitting relation	Correlation coefficient
0.3	$\phi = -0.2835e^{-0.3191t} + 0.3503$	0.9995
0.5	$\phi = -0.1699e^{-0.3705t} + 0.2354$	0.9897
0.7	$\phi = -0.0617e^{-0.2789t} + 0.1242$	0.9541
0.9	$\phi = -0.0368e^{-0.15461t} + 0.0999$	0.9274

4.2. Mass-loss effects on permeability parameters

In order to reflect the effect of mass loss on the permeability parameter, the proportional coefficient ξ is defined as the ratio of the maximum permeability parameter to the minimum permeability parameter.

$$\xi_k = \frac{k_{\max}}{k_{\min}} \tag{45}$$

where ξ_k is the proportional coefficient of permeability k, ξ_β is the proportional coefficient of non-Darcy flow β factor, ξ_c is the proportional coefficient of acceleration coefficient c_a.

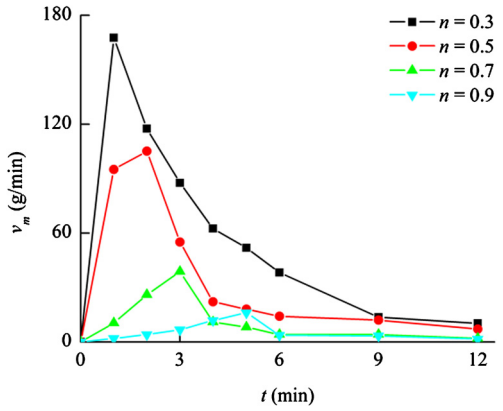

Fig. 7. Relation between mass-loss rate and time.

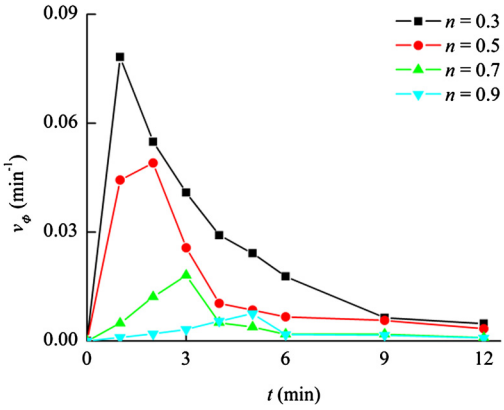

Fig. 8. Relation between porosity variation rate and time.

Fig. 9 presents the permeability–time variation curves of broken rock specimens with different Talbot gradation indices under two conditions of mass conservation and mass loss. Fig. 10 plots the maximum permeability and Fig. 11 shows the proportional coefficient ξ_k of broken rock specimens under the two conditions. It can be seen from the figures that the variation of permeability under the condition of mass conservation is caused by the migration of small particles in the internal structure of rock specimen, and the rock particles continually migrate to adjust the channels in the structure until stability. The permeability in the whole seepage process is always maintained at the same level, the maximum difference is not more than $4 \cdot 10^{-13}$ m^2. However, the broken rock specimen under the condition of mass loss is different, the permeability gradually increases in the seepage process before mutation, which is consistent with the variation law of mass loss and porosity. When the rock particles loses mass to a certain extent, the internal structures of the rock specimen cannot be enough to withstand the current conditions of external load and water erosion and then instantaneously fail, a large number of rock particles burst out with water immediately, the permeability increases exponentially. The mass loss causes the permeability of broken rock specimen to reach the maximum of $321.74 \cdot 10^{-13}$ m^2 as shown in Fig. 10. It is worth noting that the mutation time of broken rock is positively related to the Talbot gradation index. The mutation times of broken rock specimens with Talbot gradation indices of $n = 0.3$, 0.5, 0.7 and 0.9 are $t = 21$ (s), 80 (s), 127 (s), and 249 (s), respectively. The permeability increases exponentially about 200 times in a very short time (within 1–2 s), which is roughly matched with the peaks of the mass-loss rate and the porosity variation rate as shown in Figs. 7 and Fig. 8. This is similar to the study of Ma et al. [39], which pointed out that the migration of small particles has an essential effect on permeability and porosity increases during water inrush through the broken rock. In addition, it is not difficult to see from Fig. 10 and Fig. 11 that the permeability and the proportional coefficient of broken rock specimen under mass conservation are positively correlated with the Talbot gradation index; however, those are opposite under the condition of mass loss. It can be understood that more fine particles of argillaceous red sandstone are more easily combined with water molecules to form more kaolinite hydrate, which results in the volume expansion and deformation of rock particles. Under the condition of mass conservation, the rock particles cannot be lost, the volume expansion and deformation of rock particles will inevitably clog the channels in broken rock and reduce the porosity, which results in the permeability and proportional coefficient positively correlating with Talbot's gradation index. However, for the existence of mass loss, the fine rock particles gradually outflow with water causes gradual damage in the framework structure and pore structure of the broken rock. When the internal structures of broken rock cannot be enough to withstand the current conditions of external load and water erosion,

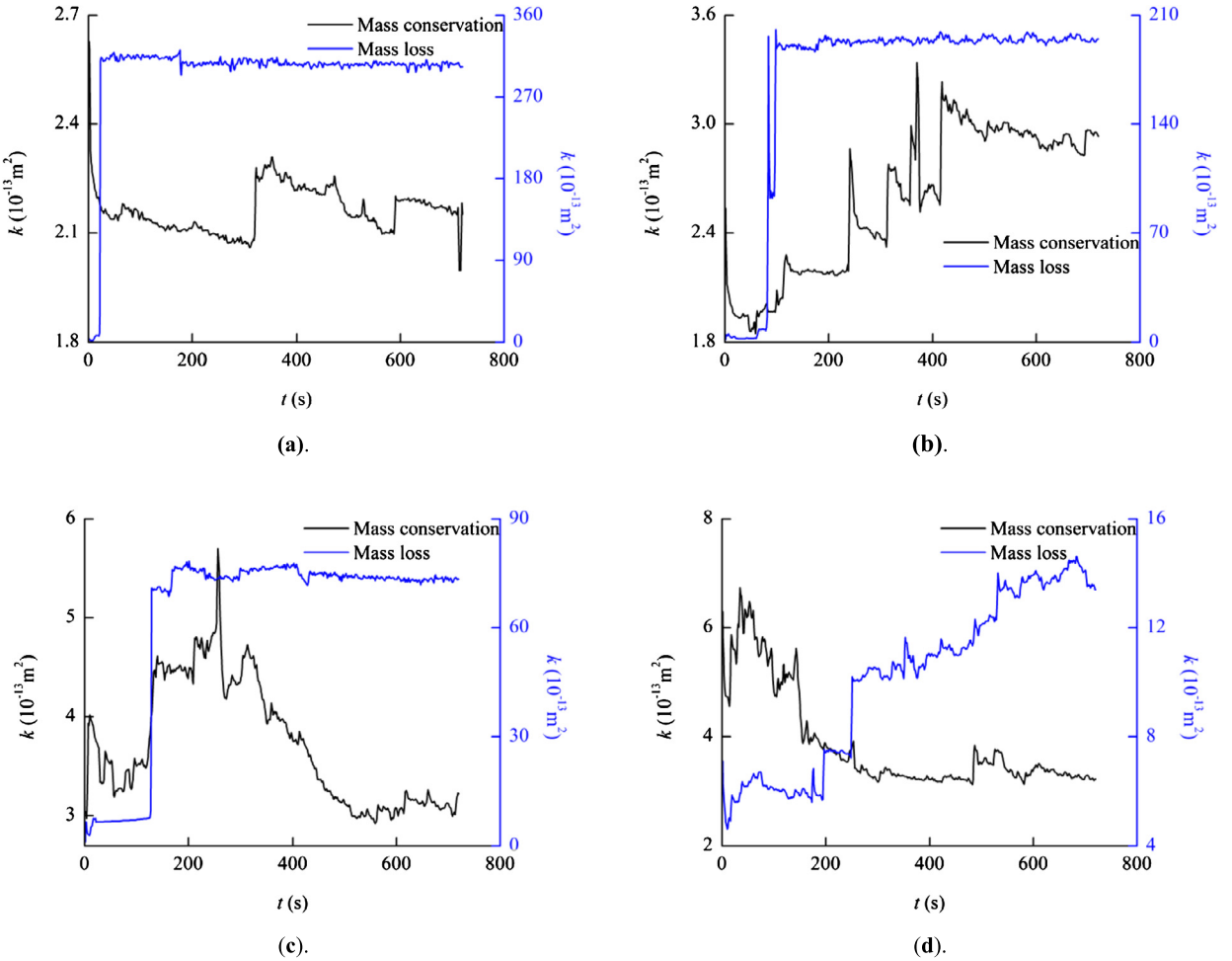

Fig. 9. Permeability–time variation curves. (**a**) $n = 0.3$; (**b**) $n = 0.5$; (**c**) $n = 0.7$; (**d**) $n = 0.9$.

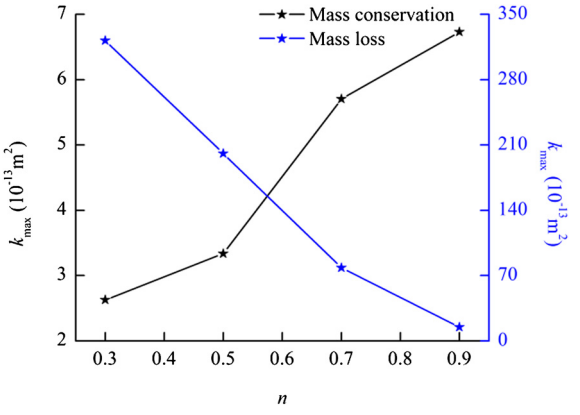

Fig. 10. Mass-loss effects on the maximum permeability.

the specimen with more small particles of argillaceous red sandstone will lose more mass. Therefore, it results in negative correlations between those two parameters and Talbot's gradation index.

During the seepage of broken rock, some studies indicated that the magnitude and history of hydraulic pressure also affected the internal structure of broken rock to present the different permeability characteristics [49,50]. Fig. 12 demonstrates the hydraulic pressure–time variation curves of broken rock specimens. The initial hydraulic pressures of all the specimens were 5 MPa, whether in terms of mass conservation or of mass loss. Under the condition of mass conservation,

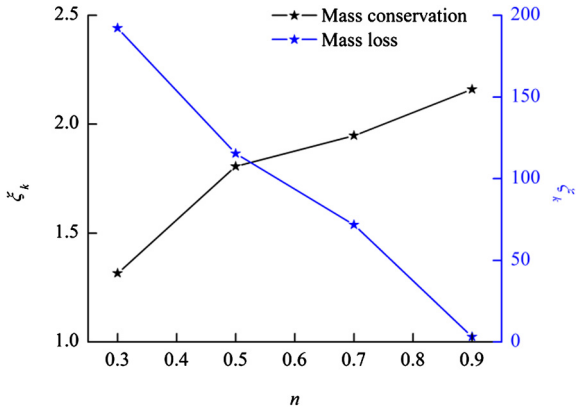

Fig. 11. Mass-loss effects on the coefficient ξ_k.

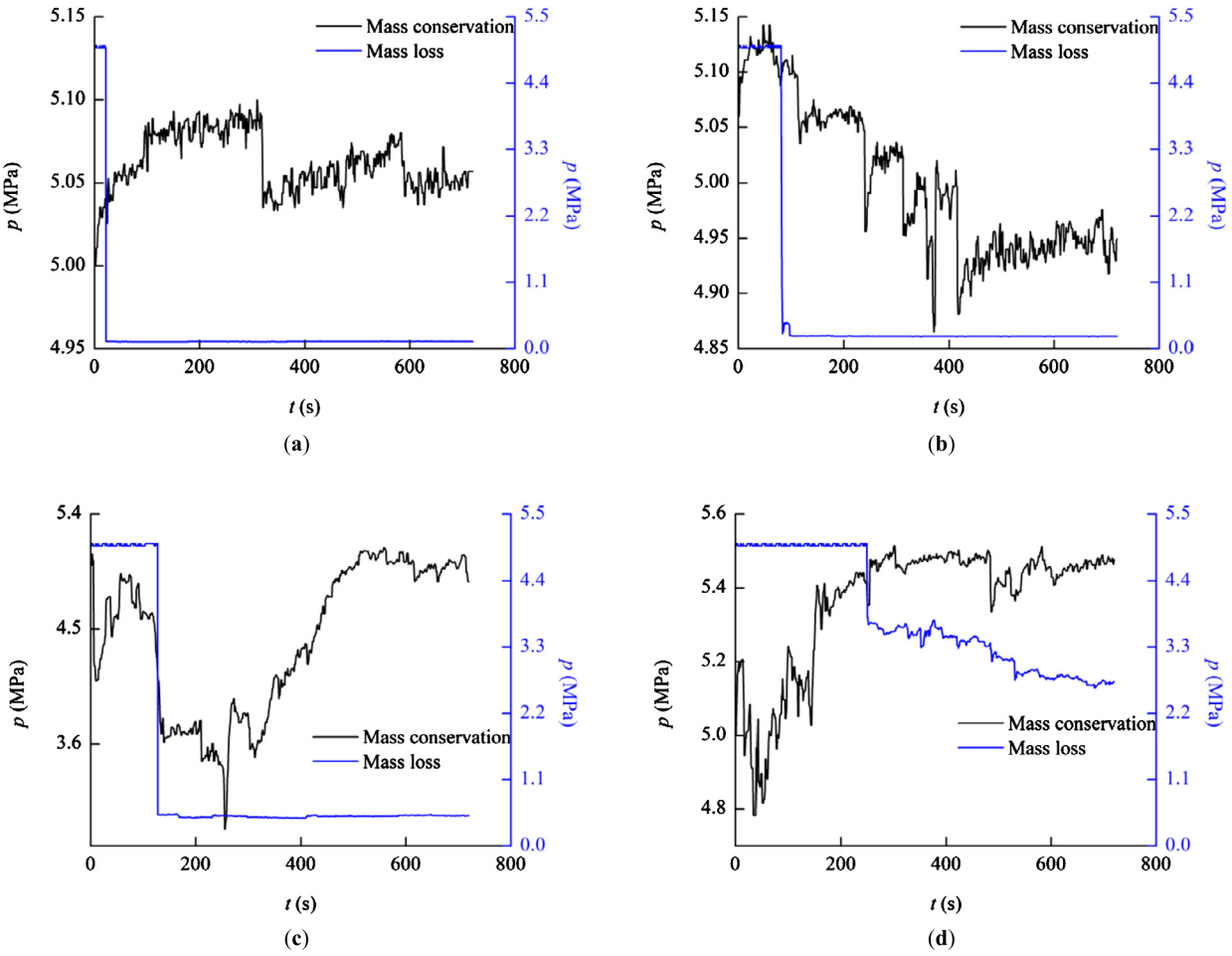

Fig. 12. Hydraulic pressure–time variation curves. (**a**) $n = 0.3$; (**b**) $n = 0.5$; (**c**) $n = 0.7$; (**d**) $n = 0.9$.

the migration of rock particles transformed the channels in the structure, which resulted in the fluctuation of hydraulic pressure. However, the fluctuation of hydraulic pressure was still maintained at around 5 MPa. In contrast, under the condition of mass loss, the hydraulic pressure dropped with the occurrence of water inrush. In the broken rock specimens with Talbot index of 0.3, 0.5 and 0.7, the hydraulic pressure instantly dropped below 0.5 MPa when the water inrush occurred. For the broken rock with a Talbot index of 0.9, its structure did not seem to be unstable, and its lost mass is the least in all the specimens. Its hydraulic pressure can still be maintained at about 2.7 MPa. Under such conditions, the flow and pressure change together, and the hydraulic pressure can vary greatly for the different tested specimens. Therefore, Marot

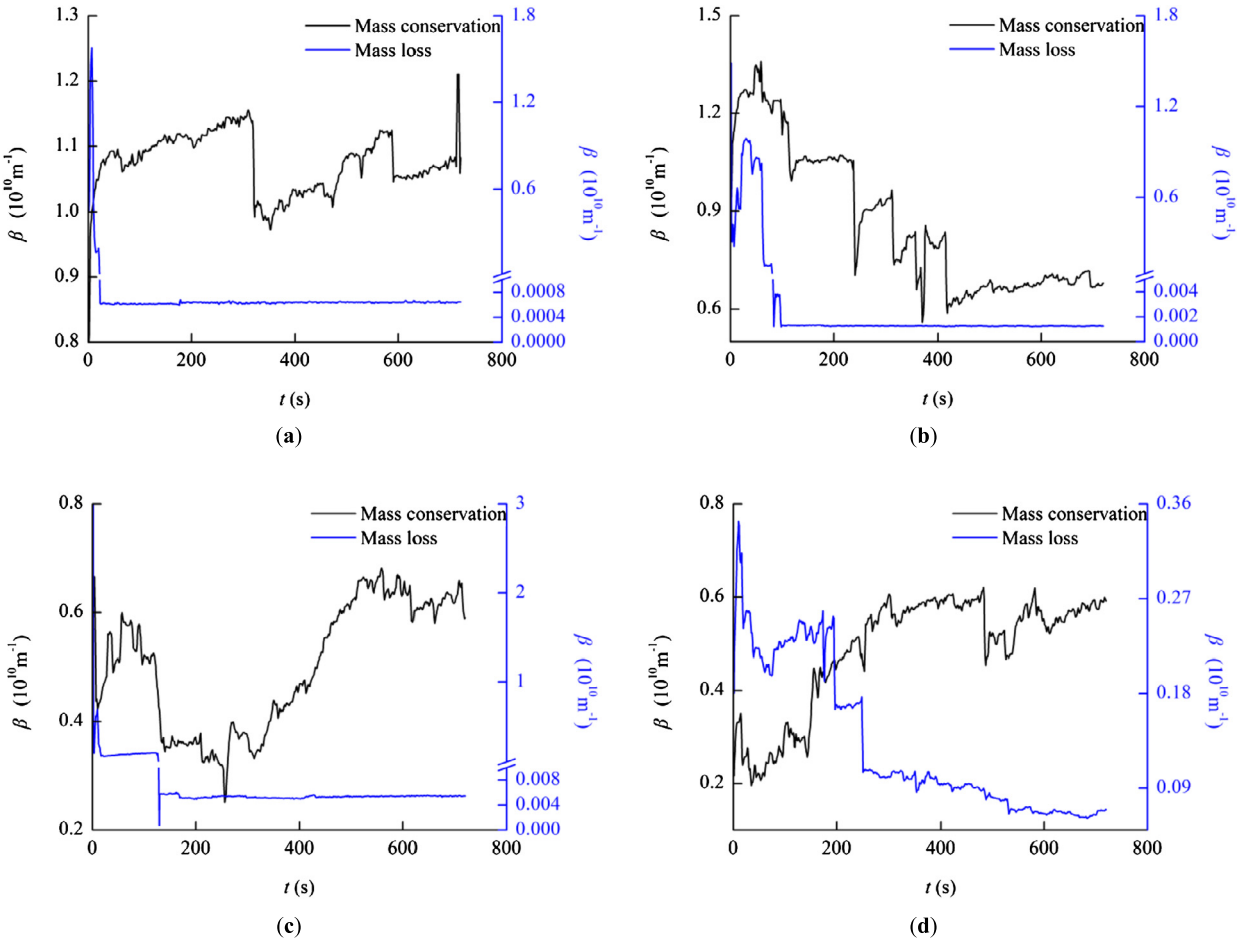

Fig. 13. Non-Darcy flow factor–time variation curves. (**a**) $n = 0.3$; (**b**) $n = 0.5$; (**c**) $n = 0.7$; (**d**) $n = 0.9$.

et al. considered that the mass loss of rock particles could be influenced by this discrepancy of hydraulic loading [51]. They suggested using the cumulative expended energy to characterize the hydraulic loading.

Fig. 13 presents the non-Darcy flow β factor–time variation curves of broken rock specimens with different Talbot gradation indices under two conditions of mass conservation and mass loss. It can be seen from the figures that the variation of the non-Darcy flow β factor is opposite to the permeability, the non-Darcy flow β factor decreasing with the increase of permeability. For the broken rock specimen under the condition of mass conservation, the migration of fine rock particles within the internal structures of broken rock also causes the fluctuation of non-Darcy flow β factor, but it remains at the same level and the maximum difference does not exceed $0.8 \cdot 10^{10}$ m^{-1}. But, for the broken rock specimen with the existence of mass loss, the non-Darcy flow β factor gradually decreases in the seepage process before mutation. When the seepage instability occurs, the mass loss causes the non-Darcy flow β factor of broken rock specimen to reach a minimum of $5.9 \cdot 10^{6}$ m^{-1}. The mutation time of the non-Darcy flow β factor is consistent with that of permeability, and the non-Darcy flow β factor also decreases exponentially about 4200 times in a very short time (within 1–2 s).

Fig. 14 presents the acceleration coefficient–time variation curves of broken rock specimens with different Talbot gradation indices under two conditions of mass conservation and mass loss. It can be seen from the figures that the variation of the acceleration coefficient is consistent with the non-Darcy flow β factor. For the broken rock specimen under the condition of mass conservation, the migration of small rock particles within the internal structures of broken rock also causes the fluctuation of acceleration coefficient, but it remains at the same level and the maximum difference does not exceed $0.7 \cdot 10^{10}$. But, for the broken rock specimen with the existence of mass loss, the acceleration coefficient gradually decreases in the seepage process before mutation. When the seepage instability occurs, the mass loss causes the acceleration coefficient of broken rock specimen to reach a minimum of $2.8 \cdot 10^{7}$. The mutation time of the acceleration coefficient is consistent with that of the non-Darcy flow β factor, and the acceleration coefficient also decreases exponentially about 800 times in a very short time (within 1–2 s).

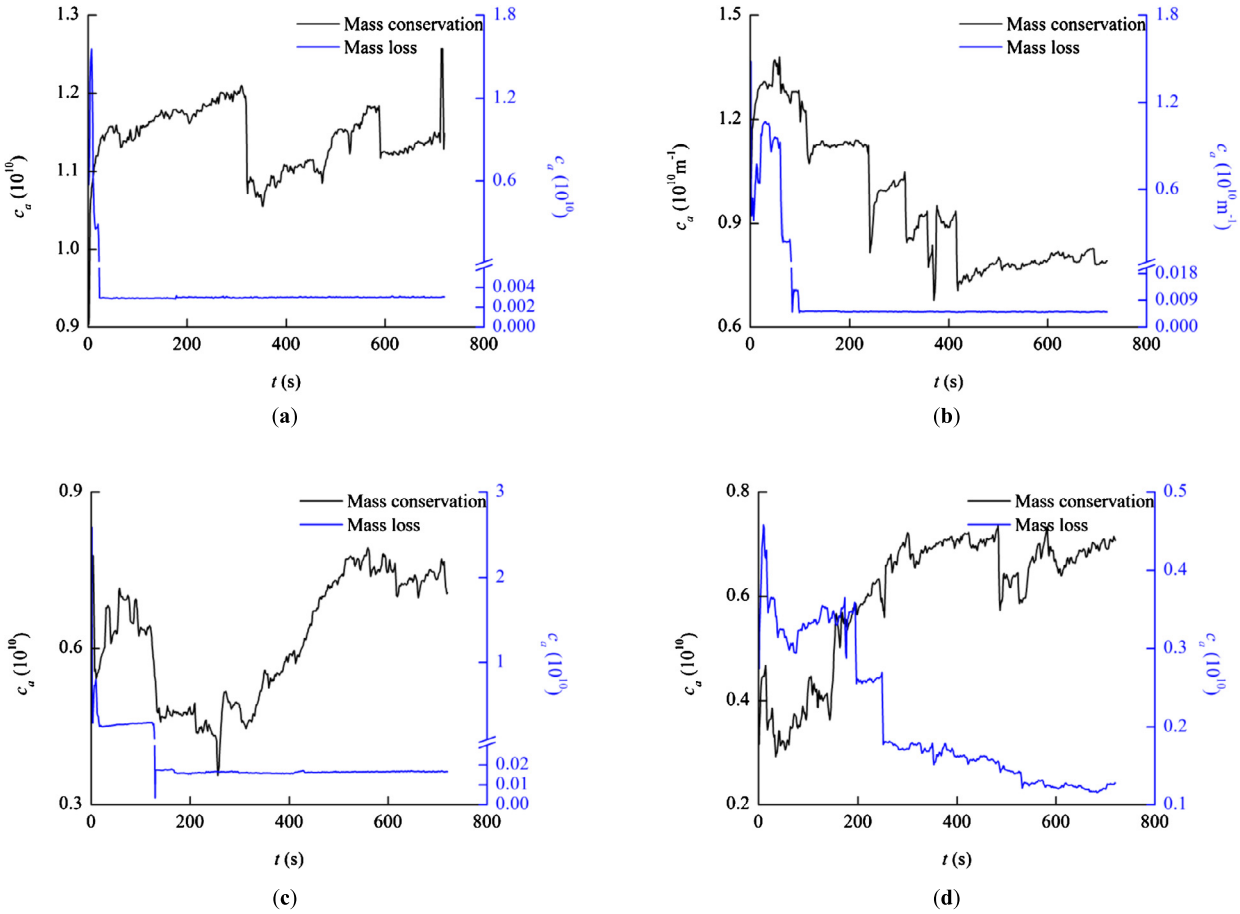

Fig. 14. Acceleration coefficient–time variation curves. (**a**) $n = 0.3$; (**b**) $n = 0.5$; (**c**) $n = 0.7$; (**d**) $n = 0.9$.

Fig. 15. Macroscopic seepage characteristic of a broken rock specimen under mass conservation.

4.3. Mass-loss effects on macroscopic seepage characteristics

Fig. 15 shows the macroscopic seepage characteristic of a broken rock specimen under the condition of mass conservation. The seepage characteristic is basically the same in the whole process, the outflow water is clear and there is no obvious fluctuation, and it matches with the characteristics of Figs. 9, 13, and 14, where the permeability parameters are always maintained at the same level under the condition of mass conservation. Fig. 16 presents the macroscopic seepage characteristics of broken rock specimens under the condition of mass loss. Fig. 17 shows the macroscopic characteristics of broken rock specimens under the condition of mass loss after seepage. A small amount of fine argillaceous red sandstones outflow with water can be seen in Fig. 16a. The channels and pore structure of the rock specimen are gradually expanded and propagated with the gradual migration and loss of rock particles, which causes more rock particles to outflow with water as shown in Fig. 16b, and the mass fraction of argillaceous red sandstone mixed with water is significantly higher

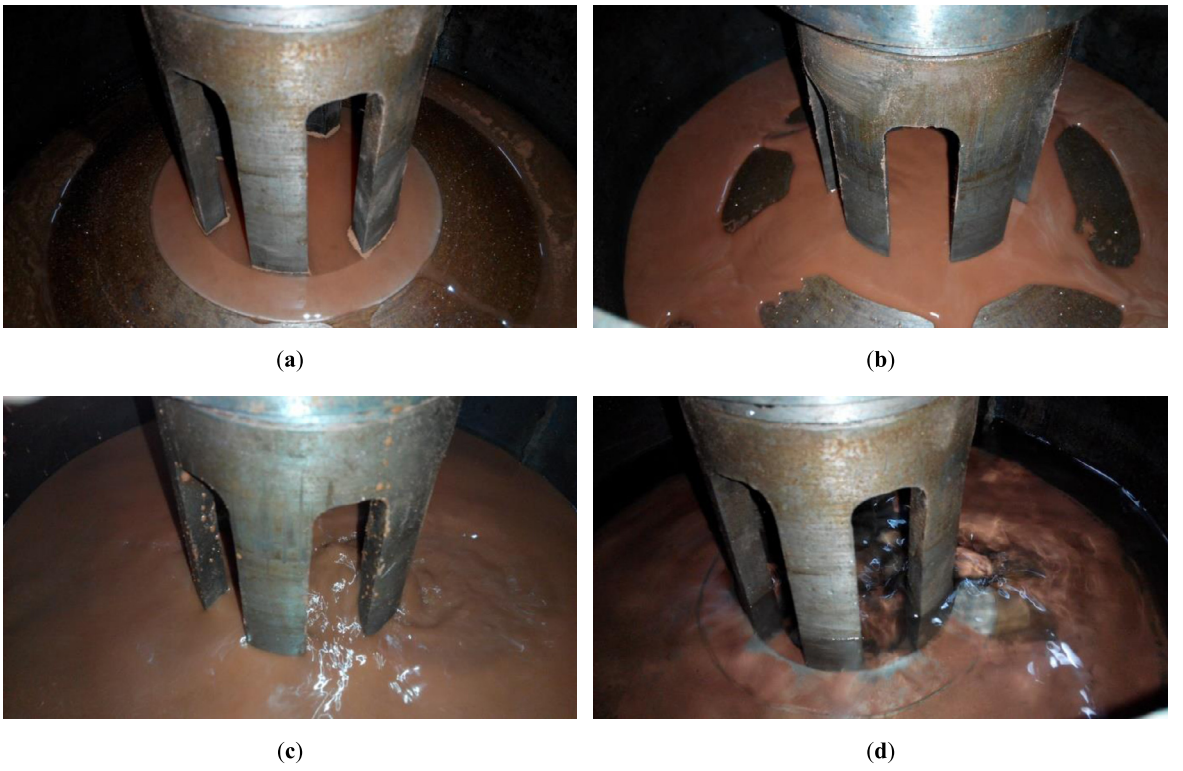

Fig. 16. Macroscopic seepage characteristics of broken rock specimen under mass loss. (**a**) Initial stage I; (**b**) initial stage II; (**c**) mutation stage; (**d**) stable stage.

than that of Fig. 16a. When the internal structures of rock specimen cannot be enough to withstand the current conditions of external load and water erosion and then instantaneously fail, the water inrush (i.e. seepage instability) occurs, a large number of rock particles burst out with water immediately, as shown in Fig. 16c. Later, due to the fact that the residual rock particles within the rock specimen have been gradually lost, the stable channels are formed in the structure, and the outflow of water is clear and no longer contains rock particles as shown in Fig. 16d. Fig. 17a and 17b show the cavities formed after the water inrush, which indicates that the flow in a broken rock specimen has been transformed from seepage to pipe flow after seepage instability. The whole seepage process is basically consistent with the various characteristics of the mass loss, porosity and permeability parameters under the condition of mass loss as shown in Figs. 7, 8, 9, 13, and 14. It is worth noting that the lost materials shown in Figs. 17c and 17d not only contain the argillization of rock particles, but also the large-scale rock particles are also easy to burst out with the gradual increase of mass loss and the gradual expansion of channels. Consequently, it results in the great deterioration of internal structure within the rock specimen and aggravates the failure caused by seepage instability.

5. Discussions

For a long time, numerous geotechnical scientists and predecessors investigated the seepage property of rock and soil mass and achieved lots of remarkable results and contributions. Darcy's flow was usually used to describe the seepage behaviors of geomaterials, which could reasonably characterize the engineering behaviors of rock and soil mass. However, in the actual project, even in the strict accordance with the geotechnical engineering safety design standards for construction, lots of engineering disasters also occurred. In the previous studies, the permeability tests on the geotechnical specimens were usually carried out based on the condition of mass conservation. Both sides of the specimen were covered with felts or filter cloths to prevent the loss of rock and soil particles. The permeability parameters obtained from these tests were used as the basic parameters of the geomaterials. Obviously, this method was largely applied in engineering with the existence of mass loss, which could not explain engineering behaviors such as the increases of porosity and permeability and even the strength deterioration of rock and soil mass caused by mass loss. Therefore, it is of great significance to discuss the influence of mass loss on the seepage property of rock and soil mass, both in theory and in engineering.

Consequently, the seepage behavior of broken rock under the condition of mass loss is presented, and the variation of the permeability parameters and macroscopic seepage characteristics can be characterized as follows.

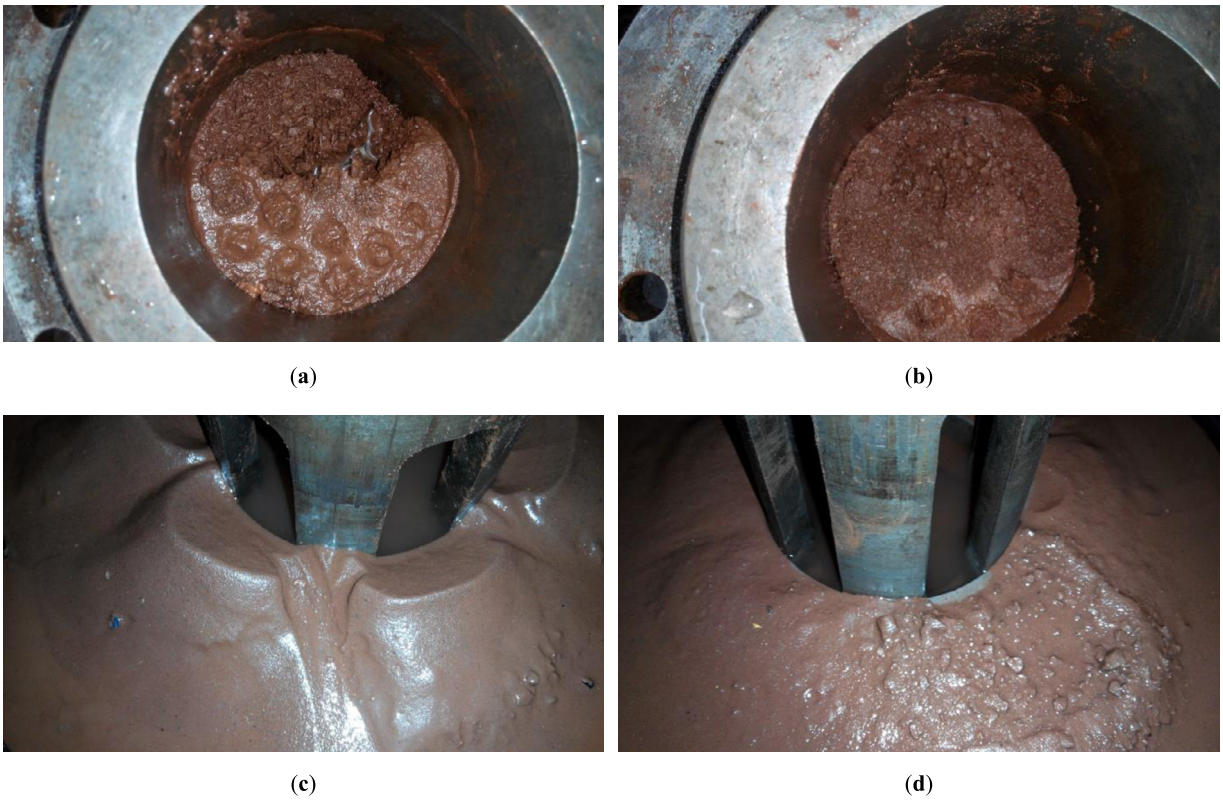

Fig. 17. Macroscopic characteristics of broken rock specimen under mass loss. (**a**) Cavities I; (**b**) cavities II; (**c**) argillization of rock particles; (**d**) large-scale rock particles.

- I. Initial stage, the gradual loss of rock particles causes the expansion and propagation of channels in the internal structures of the broken rock, and the pore structure and framework structure of the broken rock are gradually damaged, which results in the gradual variation in the seepage property of broken rock.
- II. Mutation stage, when the rock particles lose mass to a certain extent, the internal structure of the broken rock cannot be enough to withstand the current conditions of external load and water erosion, then it instantaneously fail. A large number of rock particles burst out with water immediately, which results in the mutation in the seepage property of broken rock.
- III. Stable stage, the structures are basically destructed, and the stable channels of water inrush are formed. Hereby, the seepage instability is often accompanied by structural instability.

It is reasonable to investigate the essential characteristics of engineering seepage disasters from the points of view of porosity and permeability increases and even of the strength deterioration of engineering rock caused by the existence of rock particles loss. It is worth noting that the argillaceous rock is easily corroded, eroded, and abrased under high-pressure water. Those mudding rock particles and other fine solid particles compose with water to form the two-phase fluid, which migrates in the cracks of the rock mass. And the volume fraction of those mudding and fine particles in this two-phase fluid varies with time. Due to the fact that the two-phase fluid belongs to the category of non-Newtonian fluids, the permeability of liquid and solid media is closely related to the fissure structure of the rock mass and the volume fraction of the fine particles. Therefore, in the test process, the seepage characteristics and the evolution of mass loss in broken rock specimens with different gradations presented huge differences. In the current study, it was easy to find out that the broken rock with lower Talbot index was more likely to lose the rock particles, and the produced seepage mutation was also more serious. In the results of Chang and Zhang and Indraratna et al., it was also found that the specimen with the finer particles was easier to cause the unstable structure [52,53]. It indicated that the particle size distribution of rock particles was an important factor affecting the structural stability of broken rock [54]. In addition, the effects of pore structure (porosity), stress conditions, magnitude, and history of hydraulic pressure on the broken rock also need to be evaluated [55,56].

For the seepage behavior of a broken rock under the condition of mass conservation, there is also a phenomenon due to the fact that the small fluctuation (the same level) of the permeability parameters is caused by the migration of rock particles. Obviously, both conditions of mass conservation and mass loss, the migration and loss of rock particles within broken rock inevitably cause a non-linear variation in the seepage property of the broken rock mass. Ma et al. also indicated this characteristic, and they explored the relation between the permeability and the porosity of broken rock through

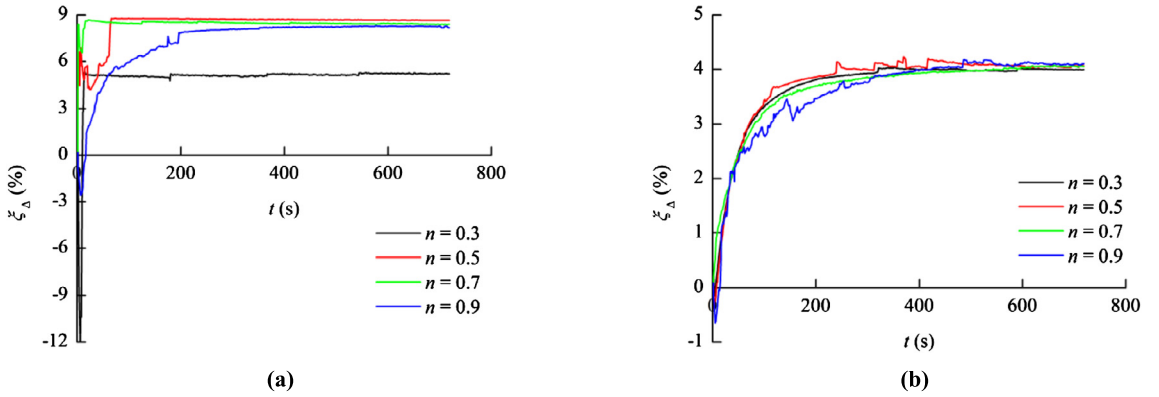

Fig. 18. Error – time variation curves. (**a**) Mass loss; (**b**) Mass conservation.

experiments under particle migration [39]. They believed that the transfer of fine particles in the broken rock mass was an important cause of mining-induced groundwater inrush. Consequently, it is important to construct a systematic algorithm for calculating the non-Darcy flow behavior to understand the nonlinear seepage characteristics of the broken rock mass [48].

The genetic algorithm of non-Darcy flow constructed in this paper can obtain the time-varying permeability parameters of broken rock. Here, it must point out the error between the calculated values and experimental values, so the error coefficient is defined as $\xi_\Delta = 1 - V'_{t_i}/V_{t_i}$. Fig. 18 shows the error per unit time (s) in the whole seepage test of broken rock under the conditions of mass loss and mass conservation. It can be seen that the errors are relatively little and that the algorithm can be used to calculate the non-Darcy flow of broken rock under mass loss or mass conservation. It should be noted that the error coefficient of broken rock under mass conservation is significantly lower than that of mass loss, and its degree of fluctuation is also significantly lower than that of mass loss. This can be understood as the effect of the destruction caused by mass loss on the internal structure of the broken rock.

It can be assumed that the mutation time of the permeability parameter substantially matches with time when the mass-loss rate and the porosity variation rate reach the peak. However, there are partial inadequacies in the above test: due to the fact that rock particles are collected once per minute, the more accurate data cannot be obtained. The presence or absence of the permeability parameters mutations advance or lag is also important to prevent the seepage instability. These parts need to be improved on this basis, including the improvement of the test system considered in the mass loss, and there will be some progress in the future. On the basis of this work, it is significant to establish an evaluation method for the mass loss of engineering rock mass and to discuss the critical conditions of seepage instability.

6. Conclusions

The experimental system for testing the seepage property of broken rock under the condition of mass loss was designed, which can also allow us to obtain the variations of mass loss and porosity. A genetic algorithm of non-Darcy flow was constructed to characterize the seepage property of broken rock. The effects of mass conservation and mass loss on the seepage properties of broken rock with different Talbot gradation indices were discussed.

(1) The loss of rock particles causes the increase of the porosity of the broken rock, and the loss mass and porosity vary with time, which can be characterized by an exponential function. The broken rock specimen with smaller Talbot gradation index loses more easily rock particles.

(2) The fluctuations of the permeability parameters under the condition of mass conservation are due to the migration of fine particles in the internal structure of the broken rock specimen, and the continuous migration of rock particles adjusts the channels in the structure until stability. The permeability parameters in the all seepage process are always maintained at the same level. But, for the broken rock specimen under the condition of mass loss, the permeability parameters gradually increase in the seepage process before mutation. When the rock particles lose mass to a certain extent, the internal structures of rock specimen cannot be enough to withstand the current conditions of external load and water erosion and then instantaneously fail, a large number of rock particles burst out with water immediately, the permeability parameters increase exponentially (permeability increases about 200 times, the non-Darcy flow β factor decreases about 4200 times and the acceleration coefficient decreases about 800 times).

(3) The permeability and the proportional coefficient ξ_k of the broken rock specimen under the conditions of mass conservation are positively correlated with the Talbot gradation index. But, for the broken rock specimen with the existence of mass loss, the permeability and the proportional coefficient ξ_k are negatively correlated with the Talbot gradation index. However, there is no obvious rule of that between the non-Darcy β factor or the acceleration coefficient and the Talbot gradation index.

(4) The loss of rock particles is an important reason for the increases of porosity and permeability and even strength deterioration in engineering rock mass with argillaceous rock. From the variation of the permeability parameters and macro-

scopic seepage characteristics, the seepage property of broken rock with the existence of mass loss can be characterized as follows.

I. The gradual loss of rock particles gradually damages the pore structure and the framework structure of the broken rock, which results in the gradual variation in the seepage property of broken rock.

II. When the rock particles lose mass to a certain extent, the internal structures of broken rock cannot be enough to withstand the current conditions of external load and water erosion and then instantaneously fail, a large number of rock particles burst out with water immediately, which results in a mutation in the seepage property of the broken rock.

III. The structures are basically destructed, and stable channels of water inrush are formed.

Acknowledgements

This work was supported by the Natural Science Foundation of Jiangsu Province (BK20160433), the National Natural Science Foundation of China (11502229), the Natural Science Foundation of the Jiangsu Higher Education Institutions of China (18KJB440002), and the Science and Technology Project of Housing and Construction in Jiangsu Province (2017ZD169).

Contributions of the authors solution

Wu Jiangyu, Han Guansheng and Feng Meimei conceived and designed the experiments; Wu Jiangyu, Han Guansheng, Gao Yuan and Yubangyong performed the experiments; Wu Jiangyu, Wang Luzhen and Kong Hailing analyzed the data; Wu Jiangyu, Han Guansheng, Feng Meimei, Gao Yuan, Yubangyong, Wang Luzhen and Kong Hailing wrote the paper.

Conflict of Interest

The authors declare no conflict of interest.

References

[1] M.H. Zhao, X.J. Zou, P.X.W. Zou, Disintegration characteristics of red sandstone and its filling methods for highway roadbed and embankment, J. Mater. Civ. Eng. 19 (5) (2007) 404–410.
[2] L. Causse, R. Cojean, J.A. Fleurisson, Interaction between tunnel and unstable slope-influence of time-dependent behavior of a tunnel excavation in a deep-seated gravitational slope deformation, Tunn. Undergr. Space Technol. 50 (2015) 270–281.
[3] T.H. Yang, T. Xu, R.Q. Rui, C.A. Tang, The deformation mechanism of a layered creeping coal mine slope and the associated stability assessments, Int. J. Rock Mech. Min. 41 (41) (2004) 827–832.
[4] T.H. Yang, P. Jia, W.H. Shi, P.T. Wang, H.L. Liu, Q.X. Yu, Seepage-stress coupled analysis on anisotropic characteristics of the fractured rock mass around roadway, Tunn. Undergr. Space Technol. 43 (7) (2014) 11–19.
[5] Z.Q. Yue, Q. Xu, Fundamental drawbacks and disastrous consequences of current geotechnical safety design theories for slopes, Chin. J. Geotechn. Eng. 36 (9) (2014) 1601–1606.
[6] D. Boldini, A. Graziani, Remarks on axisymmetric modelling of deep tunnels in argillaceous formations-II: fissured argillites, Tunn. Undergr. Space Technol. 28 (3) (2012) 80–89.
[7] N. Koronakis, P. Kontothanassis, N. Kazilis, N. Gikas, Stabilization measures for shallow tunnels with ongoing translational movements due to slope instability, Tunn. Undergr. Space Technol. 19 (4–5) (2004) 495.
[8] M.G. Sweetenham, R.M. Maxwell, P.M. Santi, Assessing the timing and magnitude of precipitation-induced seepage into tunnels bored through fractured rock, Tunn. Undergr. Space Technol. 65 (2013) 62–75.
[9] L.C. Li, T.H. Yang, Z.Z. Liang, W.C. Zhu, C.A. Tang, Numerical investigation of groundwater outbursts near faults in underground coal mines, Int. J. Coal Geol. 85 (3–4) (2011) 276–288.
[10] T.H. Yang, J. Liu, W.C. Zhu, D. Elsworth, L.G. Tham, C.A. Tang, A coupled flow-stress-damage model for groundwater outbursts from an underlying aquifer into mining excavations, Int. J. Rock Mech. Min. 44 (1) (2007) 87–97.
[11] P.L.P. Wasantha, P.G. Ranjith, Water-weakening behavior of Hawkesbury sandstone in brittle regime, Eng. Geol. 178 (8) (2014) 91–101.
[12] H.M. Tian, W.Z. Chen, D.S. Yang, F. Dai, Relaxation behavior of argillaceous sandstone under high confining pressure, Int. J. Rock Mech. Min. 88 (2016) 151–156.
[13] J.Y. Wu, M.M. Feng, B.Y. Yu, G.S. Han, The length of pre-existing fissures effects on the mechanical properties of cracked red sandstone and strength design in engineering, Ultrasonics 82 (1) (2018) 188–199.
[14] Y.H. Huang, S.Q. Yang, M.R. Hall, W.L. Tian, P.F. Yin, Experimental study on uniaxial mechanical properties and crack propagation in sandstone containing a single oval cavity, Arch. Civ. Mech. Eng. 4 (2018) 1359–1373.
[15] Z.L. Zhou, X. Cai, D. Ma, X.M. Du, L. Chen, H.Q. Wang, H.Z. Zang, Water saturation effects on dynamic fracture behavior of sandstone, Int. J. Rock Mech. Min. 114 (2019) 46–61.
[16] D.S. Yang, L.F. Chen, S.Q. Yang, W.Z. Chen, G.J. Wu, Experimental investigation of the creep and damage behavior of Linyi red sandstone, Int. J. Rock Mech. Min. 72 (2014) 164–172.
[17] Z.L. Zhou, X. Cai, D. Ma, L. Chen, S.F. Wang, L.H. Tan, Dynamic tensile properties of sandstone subjected to wetting and drying cycles, Constr. Build. Mater. 182 (2018) 215–232.
[18] P. Baud, W. Zhu, T.F. Wong, Failure mode and weakening effect of water on sandstone, J. Geophys. Res. 105 (7) (2000) 16371–16389.
[19] J. Sulem, H. Ouffroukh, Hydromechanical behaviour of Fontainebleau sandstone, Rock Mech. Rock Eng. 39 (3) (2006) 185–213.
[20] Z.H. Zhang, Q.H. Jiang, C.B. Zhou, X.T. Liu, Strength and failure characteristics of Jurassic red-bed sandstone under cyclic wetting-drying conditions, Geophys. J. Int. 198 (2) (2014) 1034–1044.
[21] J.Y. Wu, M.M. Feng, B.Y. Yu, W.L. Zhang, X.Y. Ni, G.S. Han, Experimental investigation on dilatancy behavior of water-saturated sandstone, Int. J. Min. Sci. Technol. 28 (2) (2018) 323–329.
[22] D. Ma, X. Cai, Z.L. Zhou, X.B. Li, Experimental investigation on hydraulic properties of granular sandstone and mudstone mixtures, Geofluids (2018) 9216578.

[23] W.Q. Liu, X.D. Fei, J.N. Fang, Rules for confidence intervals of permeability coefficients for water flow in over-broken rock mass, Int. J. Min. Sci. Technol. 22 (1) (2012) 29–33.
[24] X.X. Miao, S.C. Li, X.W. Huang, Experimental study of seepage properties of non-Darcy flow in granular gangues, J. China Univ. Min. Technol. 16 (2) (2006) 105–109.
[25] X.X. Miao, S.C. Li, Z.Q. Chen, Bifurcation and catastrophe of seepage flow system in broken rock, Min. Sci. Technol. 19 (1) (2009) 1–7.
[26] X.X. Miao, S.C. Li, Z.Q. Chen, W.Q. Liu, Experimental study of seepage properties of broken sandstone under different porosities, Transp. Porous Media 86 (3) (2011) 805–814.
[27] H.L. Kong, Z.Q. Chen, L.Z. Wang, H.D. Shen, Experimental study on permeability of crushed gangues during compaction, Int. J. Miner. Process. 124 (6) (2013) 95–101.
[28] D. Ma, H.Y. Duan, J.F. Liu, X.B. Li, Z.L. Zhou, The role of gangue on the mitigation of mining-induced hazards and environmental pollution: an experimental investigation, Sci. Total Environ. 664 (2019) 436–448.
[29] D. Ma, X.X. Miao, G.H. Jiang, H.B. Bai, Z.Q. Chen, An experimental investigation of permeability measurement of water flow in crushed rocks, Transp. Porous Media 105 (3) (2014) 571–595.
[30] D. Ma, X. Cai, Q. Li, H.Y. Duan, In-situ and numerical investigation of groundwater inrush hazard from grouted karst collapse pillar in longwall mining, Water 10 (9) (2018) 1187.
[31] R.C. Liu, B. Li, L.Y. Yu, Y.J. Jiang, H.W. Jing, A discrete-fracture-network fault model revealing permeability and aperture evolutions of a fault after earthquakes, Int. J. Rock Mech. Min. 107 (7) (2018) 19–24.
[32] W.G. Liang, Y.S. Zhao, S.G. Xu, M.B. Dusseault, Dissolution and seepage coupling effect on transport and mechanical properties of glauberite salt rock, Transp. Porous Media 74 (2) (2007) 185–199.
[33] R.C. Liu, B. Li, Y.J. Jiang, L.Y. Yu, A numerical approach for assessing effects of shear on equivalent permeability and nonlinear flow characteristics of 2-D fracture networks, Adv. Water Resour. 111 (2018) 289–300.
[34] R.C. Liu, B. Li, Y.J. Jiang, A fractal model based on a new governing equation of fluid flow in fractures for characterizing hydraulic properties of rock fracture networks, Comput. Geotech. 75 (5) (2016) 57–68.
[35] K. Zhang, B.Y. Zhang, J.F. Liu, D. Ma, H.B. Bai, Experiment on seepage property and sand inrush criterion for granular rock mass, Geofluids (2017) 9352618.
[36] R.C. Liu, Y.J. Jiang, B. Li, X.S. Wang, A fractal model for characterizing fluid flow in fractured rock masses based on randomly distributed rock fracture networks, Comput. Geotech. 65 (4) (2015) 45–55.
[37] B.Y. Yu, Z.Q. Chen, Q.L. Ding, L.Z. Wang, Non-Darcy flow seepage characteristics of saturated broken rocks under compression with lateral constraint, Int. J. Min. Sci. Technol. 26 (6) (2016) 1145–1151.
[38] T. Yuan, Y. Ning, G. Qin, Numerical modeling and simulation of coupled processes of mineral dissolution and fluid flow in fractured carbonate formations, Transp. Porous Media 114 (3) (2016) 747–775.
[39] D. Ma, M. Rezania, H.S. Yu, H.B. Bai, Variations of hydraulic properties of granular sandstones during water inrush: effect of small particle migration, Eng. Geol. 217 (1) (2017) 61–70.
[40] M.M. Feng, J.Y. Wu, D. Ma, X.Y. Ni, B.Y. Yu, Z.Q. Chen, Experimental investigation on seepage property of saturated broken red sandstone of continuous gradation, Bull. Eng. Geol. Environ. 77 (3) (2018) 1167–1178.
[41] M.M. Feng, J.Y. Wu, Z.Q. Chen, X.B. Mao, B.Y. Yu, Experimental study on the compaction of saturated broken rock of continuous gradation, J. China Coal Soc. 41 (9) (2016) 2195–2202.
[42] L. Qiao, P.G. Ranjith, X.P. Long, Y. Kang, M. Huang, A review of shale swelling by water adsorption, J. Nat. Gas Sci. Eng. 27 (2015) 1421–1431.
[43] ASTM Standard C192/C192M-13a, Standard practice for making and curing concrete test specimens in the lab. annual book of ASTM standards, West Conshohocken, PA. Available online: https://doi.org/10.1520/C0192_C0192M-13A, 2013.
[44] J.Y. Wu, M.M. Feng, X.B. Mao, W.L. Zhang, X.Y. Ni, G.S. Han, Particle size distribution of aggregate effects on mechanical and structural properties of cemented rockfill: experiments and modeling, Constr. Build. Mater. 193 (2018) 295–311.
[45] P.H. Forchheimer, Wasserbewegun durch Boden, Z. Ver. Dtsch. Ing. 49 (1901) 1736–1749 and 50, 1781–1788.
[46] S. Irmay, On the theoretical derivation of Darcy and Forchheimer formulas, J. Geophys. Res. 39 (4) (1958) 702–707.
[47] T. Giorgi, Derivation of the Forchheimer law via matched asymptotic expansions, Transp. Porous Media 29 (2) (1997) 191–206.
[48] L.Z. Wang, H.L. Kong, Variation characteristics of mass-loss rate in dynamic seepage system of the broken rocks, Geofluids 7137601 (2018).
[49] Y.L. Luo, L. Qiao, X.X. Liu, M.L. Zhan, J.C. Sheng, Hydro-mechanical experiments on suffusion under long-term large hydraulic heads, Nat. Hazards 65 (3) (2013) 1361–1377.
[50] A. Rochim, D. Marot, L. Sibille, V.T. Le, Effect of hydraulic loading history on the characterization of suffusion susceptibility of cohesionless soils, J. Geotech. Geoenviron. Eng. 143 (7) (2017) 04017025.
[51] D. Marot, A. Rochim, H.H. Nguyen, F. Bendahmane, L. Sibille, Assessing the susceptibility of gap graded soils to internal erosion: proposition of a new experimental methodology, Nat. Hazards 83 (1) (2016) 365–388.
[52] D.S. Chang, L.M. Zhang, Extended internal stability criteria for soils under seepage, Soil Found. 53 (4) (2013) 569–583.
[53] B. Indraratna, J. Israr, C. Rujikiatkamjorn, Geometrical method for evaluating the internal instability of granular filters based on constriction size distribution, J. Geotech. Geoenviron. Eng. 141 (10) (2015) 04015045.
[54] E. Vincens, K.J. Witt, U. Homberg, Approaches to determine the constriction size distribution for understanding filtration phenomena in granular materials, Acta Geotech. 10 (3) (2015) 291–303.
[55] D.S. Chang, L.M. Zhang, A stress-controlled erosion apparatus for studying internal erosion in soils, Geotech. Test. J. 34 (6) (2011) 579–589.
[56] R.C. Liu, B. Li, Y.J. Jiang, Critical hydraulic gradient for nonlinear flow through rock fracture networks: the roles of aperture, surface roughness, and number of intersections, Adv. Water Resour. 88 (2) (2016) 53–65.